Conference Proceedings

Solar World Congress 2015
Daegu, Korea, 08 – 12 November 2015

Solar thermal energy performance model for an interactive solar energy atlas for the Arabian Peninsula

Mercedes Ibarra[1], Miguel Frasquet[1], Abdulaziz Al Rished[2], Arttu Tuomiranta[1], Sami Gasim[2] and Hosni Ghedira[1]

[1] Masdar Institute of Science and Technology, Research Center for Renewable Energy Mapping and Assessment (ReCREMA), P.O. Box 54224, Abu Dhabi, United Arab Emirates

[2] King Abdullah City for Atomic & Renewable Energy (KACARE), P.O. Box 2022, Riyadh 11451, Saudi Arabia

Abstract

The authors present the integration of a solar thermal energy performance model in an already existing solar atlas infrastructure. With this tool, the user will be able to select the design parameters of a solar power plant and the key performance indicators will be delivered. In particular, this paper presents the two performance models proposed to assess the performance of utility-scale solar thermal power plants. The results of these models have been used for the evaluation of the potential of solar energy in the Arabian Peninsula.

Keywords: *solar thermal energy (STE), simulation, parabolic trough collector (PTC), central receiver systems (CRS).*

1. Introduction

Until now, countries like Saudi Arabia and UAE have based their energy consumption on its great resources of oil and gas. However, the Middle East is a region with high solar energy potential. The use of solar energy to produce electricity instead of burning fossil fuels would have several advantages, like avoiding consuming a well valued resource, and reducing the dependence of a finite resource.

To impulse the development of solar energy projects, KACARE proposed the development of a solar atlas, where the solar irradiance potential would be offered to the general public. The website is online and operational (KACARE, 2015). Moreover, a joint project between ReCREMA and KACARE aims to include a solar technology assessment layer into the atlas, where the performance of several solar technologies will be available. The technologies included in the solar simulator will be photovoltaic solar energy (PV) and solar thermal energy technologies, like parabolic trough collectors (PTC) and central receiver systems (CRS).

In this paper, the models used in the solar simulator for the solar thermal technologies are presented and compared. The spatial aspects of the simulation are analyzed to improve the speed and performance of the simulator. As an example of the capabilities of the model, two plants are designed and their annual performance is calculated.

2. General overview of the solar atlas operation

There are three kinds of inputs for the solar technology assessment atlas: the user defines the major characteristics of the plant (i.e. design net output power, solar multiple and hours of storage), the pixels on the map states the location-related information and the fixed inputs are logic design assumptions specified in the model to simplify it and avoid long computation times, benchmarked with industrial standards.

Once the inputs are defined, the model performs two calculations for each pixel of the map. First, the layout of the plant is determined. Then, the tool estimates the annual performance of the plant.

doi:10.18086/swc.2015.04.20 Available at http://proceedings.ises.org

3. Performance models

3.1. CRS Model

During the first step of the design point evaluation, a detailed power block model is used to calculate the required power at the steam generator. This power block model simulates a 50-100 MWe state of the art steam Rankine cycle. Bigger sizes would imply a significant drop of the optical efficiency due to the extreme atmospheric attenuation in the Arabian Peninsula.

Therefore, sizes bigger than 100 MWe are assumed as multiples of the power block model. The partial load behavior is also modeled assuming sliding pressure control, and performance maps are created to be implemented in the annual performance calculations. Knowing the power absorbed at the steam generator and the solar multiple (defined by the user), the power absorbed by the receiver can be estimated. Using this value and the information provided by each pixel (design direct normal irradiance and latitude), the height of the tower and the size of the receiver are optimized through pre-calculated DELSOL3 optimizations. The optimization has been done with the economic parameters incorporated, although the user will not be able to change the values. In this optimization, the pre-calculated data is limited to 105 possibilities for each variable and the rest of the possible combinations are interpolated from the data.

The layout of the solar field cannot be obtained by interpolation and therefore, it should be calculated for each case. For that purpose, a complete optical model in MATLAB has been developed. This optic model discretizes the field using a cell pattern similar to DELSOL3 approach, and takes into account the optical behavior of each cell. The shadowing and blocking (S&B) engine uses an intelligent neighbor selector and the classic approach of surface projection. Fig. 1 shows the validation results of the S&B engine proposed, against a ray-tracing code and its evolution along the year.

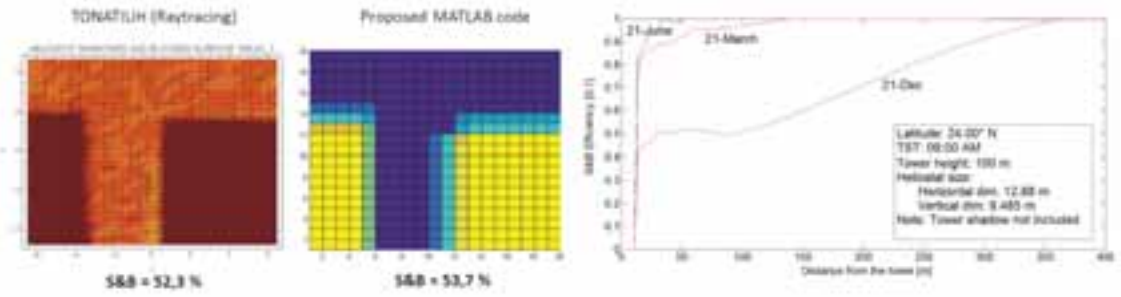

Fig. 1: S&B validation of the proposed code in MATLAB using Tonatiuh Raytracing

The evaluation of the flux at the receiver necessary to determine the spillage, is numerically calculated using a circular Gaussian approach similar to the one used in HFLCAL. The computer program HFLCAL was developed by Michael Kiera at the German company Interatom during the project GAST (GAS-cooled Solar Tower) in the early 1980's (Kiera, 1989). Once the optical efficiencies are calculated, the optical model re-arranges the cells and calculates the optimum field layout.

The size of the receiver is interpolated from the pre-calculated DELSOL3 optimization data and introduced into a thermodynamic receiver model. The receiver model calculates the thermal efficiency of the receiver as well as other outputs needed for the overall model e.g. molten salts mass flow rate, salts-pump consumption. The partial load behavior is also calculated and represented in a set of performance maps which will be used in the annual performance model.

The Fig. 2 shows an example of the solar field created by the model. The rather circular geometry agrees with the DELSOL3 optimizations and reflects the fact that in areas with a significant atmospheric attenuation, as the case of the Arabian Peninsula, circular fields are preferred against North/South fields. This field creation takes into account energy performance and economic parameters. If only the energy performance were taken into account, the resulted solar field will have very high tower with big receivers

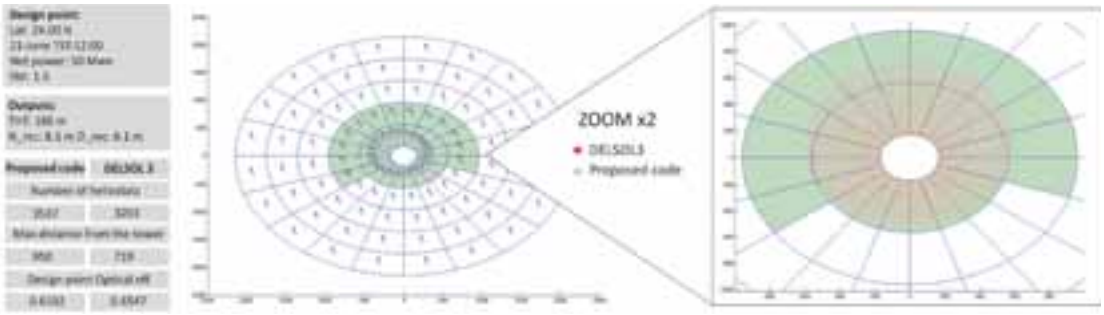

Fig. 2: Solar field layout created by the proposed model

3.2. PTC Model

The PTC plant design, which is defined by the spatial organization of the collectors, is easier to determine. The PTC collectors are arranged in loops of collectors in series. Ideally, every loop receives the same irradiance and heats a fraction of the thermal oil by the same temperature difference. Hence, the aperture area of a PTC solar field depends on the desired power, the available incident power (Q_{sun}) and the performance of one loop to transform this incident power in thermal energy.

Therefore, the calculation of the efficiency of one loop in design conditions is needed to design the power plant. To do so, first the amount of energy available for the loop and then the optical and thermal losses of the collector are calculated. Once the plant design is determined, the annual performance of the plant can be simulated. For every time step, the simulator uses the meteorological database associated to the pixel to follow the same step than for the design.

First, the available incident power (Q_{sun}) is defined by the following expression:

$$Q_{sun} = \mathrm{G_b} \cdot \cos\theta_i \cdot A_{apert} \qquad \text{(eq. 1)}$$

where G_b is the direct irradiance, θ_i is the incidence angle and A_{apert} is the aperture area of the solar field.

Then, the absorbed energy by the collector tube is calculated following the guidelines proposed by the GuiSMo project Eck et al. (2014) that recommends including accurate optical efficiency information of the collector, the incidence angle modifier (IAM), the end losses and the shading effects.

The optical efficiency is calculated by eq.2. It is assumed that the solar field is periodically cleaned and that the value of F_d (cleanliness factor) changes randomly among certain values that follow a normally distributed function, and so do the reflectivity of the mirrors, the transmissivity of the tube cover and the absorptivity of the tube. This method was proposed by Zaversky et al. (2012) and the values used are based on the SEGS experimental data.

$$\eta_{opt,0^\circ} = r_{0^\circ} \cdot \gamma_{0^\circ} \cdot \tau_{0^\circ} \cdot \alpha_{0^\circ} \cdot F_{d,0^\circ} \qquad \text{(eq. 2)}$$

where r_0 is the reflectivity of the parabolic mirrors, γ_0 is the geometric intercept factor of the collector, τ_0 is the transmissivity of the receiver's glass cover and α_0 is the absorbance of the selective coating on the metallic pipe, all at θ=0º.

The IAM is determined by:

$$\mathrm{K}(\theta) = 1 - \mathrm{a_0} \cdot \theta - \mathrm{a_1} \cdot \theta^2 + \mathrm{a_2} \cdot \theta^3 + \mathrm{a_3} \cdot \theta^4 \qquad \text{(eq. 3)}$$

where θ is the incidence angle and the coefficients used are a_0=2.2307·10^{-4}, a_1=1.1·10^{-4}, a_2=3.18596·10^{-6} and a_3=-4.85509·10^{-8}.

The end losses (f_{end}) and the shading effects ($f_{rowShadow}$) are calculated following the equations, from Eck et al. (2014):

$$f_{end} = 1 - {f_m \cdot \tan\theta}/{l_{col}} \qquad \text{(eq. 4)}$$

$$f_{rowShadow} = \max\left[0, \min\left[1, \frac{d_{row}}{w_{col}} \frac{\sin\alpha_s}{\cos\theta}\right]\right] \quad \text{(eq. 5)}$$

where l_{col} and w_{col} is the length and width of the collector, d_{row} is the distance between rows, f_m is the focal length of the parabola and α_s is the solar altitude.

The energy absorbed by the tube is defined as:

$$Q_{abs} = Q_{sun} \cdot IAM \cdot \eta_{\text{opt},0^\circ} \cdot f_{end} \cdot f_{shadow} \quad \text{(eq. 6)}$$

The receiver thermal losses are calculated following the regression lines obtained by Burkholder et al. (2008) for the Schott PRT70:

$$H_L = b_0 + b_1 \cdot (T_{HTF} - T_{amb}) + b_2 \cdot {T_{HTF}}^2 + b_3 \cdot {T_{HTF}}^3 + b_4 \cdot G_b \cdot \cos\theta \cdot {T_{HTF}}^2 + \\ + \sqrt{V_w} \cdot (b_5 + b_6 \cdot (T_{HTF} - T_{amb})) \quad \text{(eq. 7)}$$

where T_{HTF} is the temperature of the fluid, T_{amb} is the ambient temperature, V_w is the wind speed and the coefficients are shown in Tab. 1.

Tab. 1: Values of the coefficients for the heat losses calculations (Burkholder, 2008).

b_0	4.05
b_1	0.247
b_2	-0.00146
b_3	5.65E-6
b_4	7.62E-8
b_5	-1.70
b_6	0.0125

The thermal losses of the piping are calculated following the method proposed by Patnode (2006):

$$H_{L,Pip} = c_0 \cdot (T_{HTF} - T_{amb}) + c_2 \cdot (T_{HTF} - T_{amb})^2 + c_3 \cdot (T_{HTF} - T_{amb})^3 \quad \text{(eq. 8)}$$

where c_0=1.693·10^{-2}, c_1=1.683·10^{-4}, c_3=6.78·10^{-7}.

Once the amount of thermal energy provided by the solar field is calculated, the control algorithm determines the amount of energy sent to the power block and thermal storage.

For the determination of the efficiency and power production of the power block the model uses the equation proposed by Llorente et al. (2011).

$$\eta_{PB} = a_1 + a_2 \cdot \exp\left(-P_{in}/a_3\right) \quad \text{(eq. 9)}$$

where the P_{in} is the power delivered to the power block after the heat exchanger (η_{HEX}=0.95), a_1 = 0.397, a_2 = -0.243 and a_3 = 28.23 MWt

The model is compared with the performance of a solar plant located in similar desert conditions: the 100 MW Shams 1 solar plant, operated by Shams Power Company, owned by Masdar, Total and Abengoa, located in Madinat Zayed (UAE). The solar field has 627,840 m^2 of parabolic trough, divided in four section. The particularity of the design of this plant was the addition of a gas booster before the turbine, to increase the steam temperature the feeds it, which allows an increase of the efficiency of the turbine.

The data used, provided by Shams Power Company, has allowed the comparison of the power output from the solar field (before going to the power block) for the same conditions (DNI and ambient temperature) and compared with the actual values obtained in the field. Due to the particular configuration of the power block, the power production could not be included in the comparison. The scatter density plot of the measured

($P_{SF,meas}$) and predicted solar field power ($P_{SF,mod}$) is shown in Fig. 3, where the correspondence of the model values with the measured is good with a slight overestimation of the production in the model for lower values.

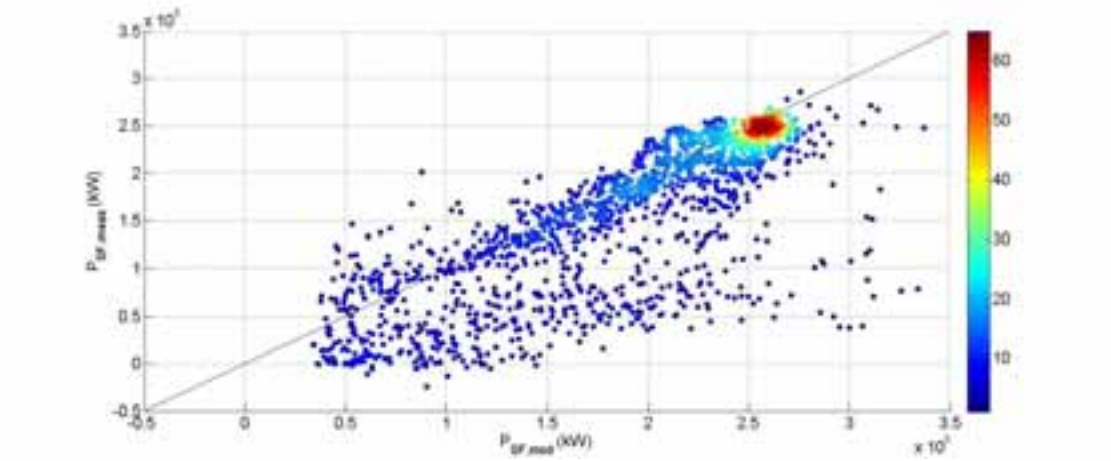

Fig. 3: Scatter density plot for power measured and power predicted by the model

4. Preliminary results

4.1. Geographic influence on the design of power plants

In this work, the presented models have been used to analyze the effect of the geography distribution of the input variables (G_b, solar angles) on the final design of the plants.

In Fig. 4 a map of the distributions of the direct solar irradiance G_b in 2013 of Saudi Arabia is shown. The country is located between the parallels 35 and 15 in the northern hemisphere, which means almost 15° of amplitude. This great extension affects the distribution of the DNI, with an increasing gradient that goes from north to south. However, the greater values are found at the west of the country, by the coast.

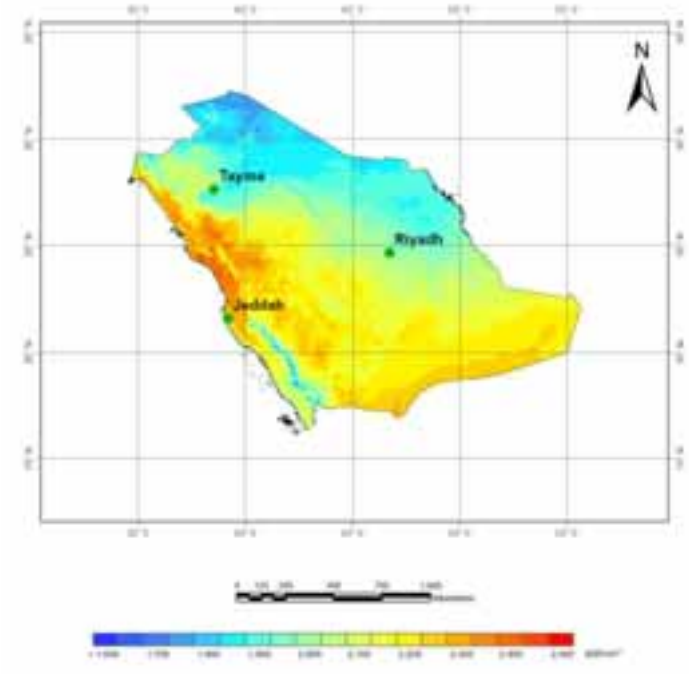

Fig. 4: Beam irradiance on Saudi Arabia on 2013

In Fig. 5 and 6 the effect of the design beam irradiance and the latitude on the design of the plants is shown. The latitude affects the position of the sun in relation to the the collectors or heliostats and it therefore has an impact on the incidence angle value. The southern the location, higher the sun will reach in the sky and smaller the incidence angle will be. As a consequence of this, the smaller the latitude (south), the smaller the area required to reach the desired power in the design conditions. Regarding the height of the tower, it gets taller when going south because the solar angles allow circle shaped heliostat field. This means that the heliostats are closer and the tower is higher.

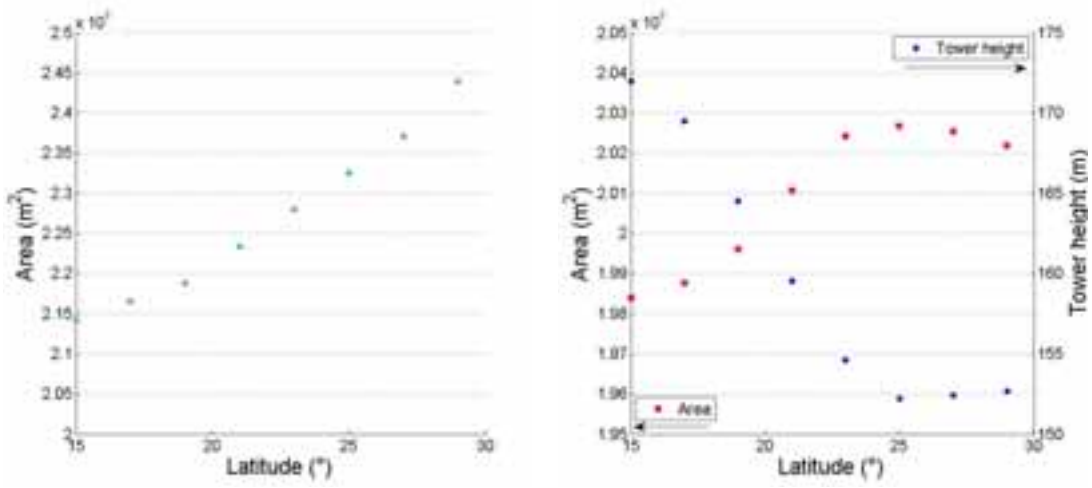

(a) (b)

Fig. 5: Effect of the latitude on the design of the plant (a) PTC and (CRS)

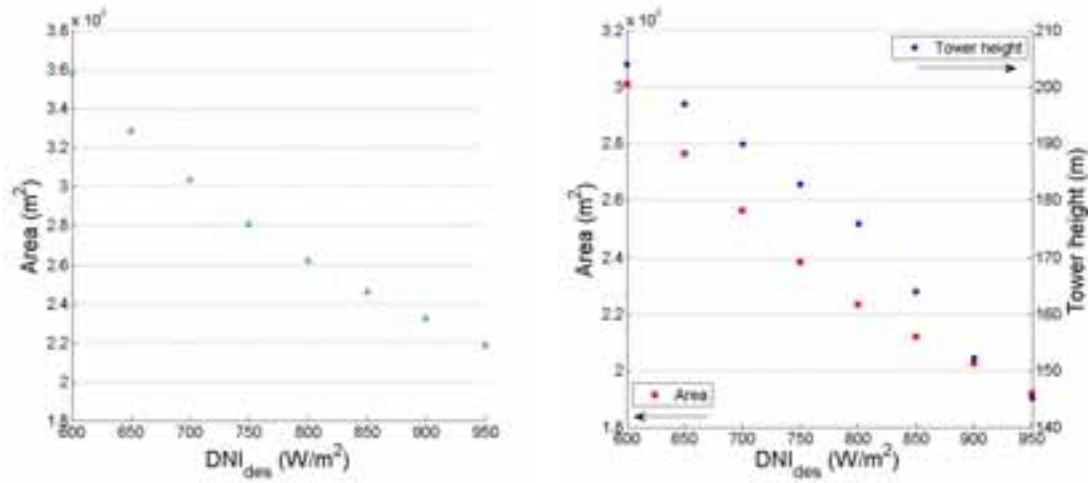

(a) (b)

Fig. 6: Effect of the design beam irradiance on the design of the plant (a) PTC and (CRS)

Regarding the effect of the DNI (Fig) has on the design, the greater the DNI, smaller area will be needed to cover the desired power on the design conditions. Hence, the higher the DNI, the smaller the plant will be. Again, this means that as we go south in the country, the required area will be smaller.

As the DNI values and solar angles are no constant along the year, the choice of the design point (DNI and solar angles) will affect the performance of the plant. If a winter design date is chosen, the plant will be overdimensioned and most of the time the plants will be producing more energy that what they were designed for, having to dump most of this energy by defocusing. If a summer design date is chosen, the plant may be underdimensioned, producing under the desired power for most of the year.

4.2. Case study: design of a plant in Riyadh

The models presented in the previous section have been used to design two plants in Riyadh, which has a latitude of 24.53° and a beam irradiance on design of 843.9 W/m^2. The results of this exercise are shown in Tab.1.

Tab. 1: Comparison of the designed plants for Riyadh

Design point	Design CRS	Design PTC
Latitude: 24.53N	Tower Height: 186 m	Collectors per loop: 4
Longitude: 46.44E	Dimension receiver: 8.1 x 6.1 m^2	Number of loops: 151
21-June solar noon	Number heliostats: 3537	Total number SCA: 604
Design net power: 50MWe	Max distance of the tower: 950 m	Aperture area: 3.44 ·10^5 m^2
SM:1.5	Optical efficiency: 0.6102	

Fig. 7 and 8 show the summary of the simulation for the two solar fields of Tab. 1: each square represents the hourly average power delivered by the solar field of every month. The DNI resource is the same for both technologies, the months with less resource being March, April and May.

However, the production of the CRS solar field is more constant through the year than PTC solar field one. The reason of for this difference divergence discrepancy is the different in incidence angle between the two technologies. In winter, when the sun is lower, the PTC optical efficiency decreases more significantly due to single-axis tracking.

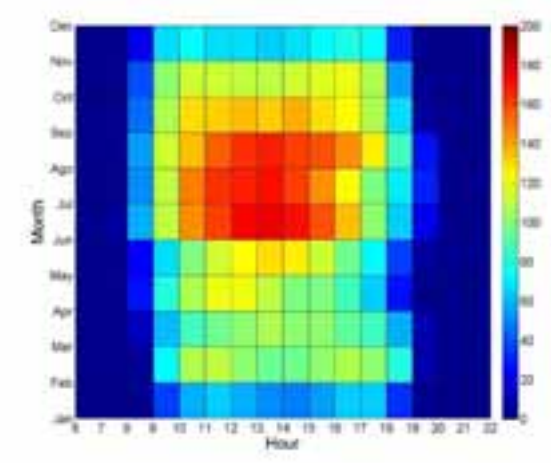

Fig. 7: Average power delivered to the power block by the parabolic trough collector solar field for every hour of every month

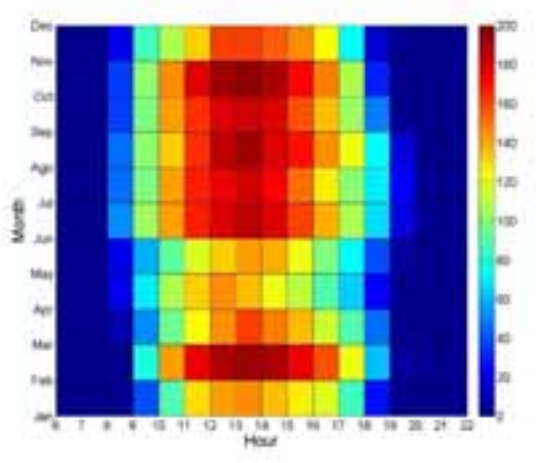

Fig. 8: Average power delivered to the power block by the central receiver system (heliostats and receiver) for every hour of every month

5. Conclusions

This paper presents the model used in a solar technology atlas for Saudi Arabia. The models for two technologies are presented: PTC and CRS. Both models are validated, either with real operational data or from widely accepted industry codes. In this work, a special focus has been given to the design step of the calculations.

Therefore, the presented models have been used to analyze the effect of the geography distribution of the input variables on the final design of the plants. The southern the location, both the beam irradiance and the solar angles values allow the reduction of the area of the solar field to reach the same power. Moreover, due to the

solar angles in low latitudes, in the case of the CRS the tower gets higher and the heliostat field design will be more compact.

As a final step, two plants have been designed in Riyadh and their annual performance has been calculated. A more stable thermal energy is delivered to the power block in the case of CRS, being the PTC more variable seasonably.

6. References

Burkholder, F., Kutscher, C., 2008a. Heat-Loss Testing of Schott's 2008 PTR70 Parabolic Trough Receiver. NREL TP-550-42394, pp. 1–54.

Eck, M., T. Hirsch, J.F. Feldho, D. Kretschmann, J. Dersch, A. Gavilan Morales, L. Gonzalez-Martinez, C. Bachelier, W. Platzer, K.-J. Ri_elmann, and M. Wagner. Guidelines for csp yield analysis. optical losses of line focusing systems; definitions, sensitivity analysis and modeling approaches. Energy Procedia, 49(0):1318 - 1327, 2014. Proceedings of the SolarPACES 2013 International Conference.

K.A.CARE, Renewable Resource Atlas. http://rratlas.kacare.gov.sa. Accessed on 26/Oct/2015.

Kiera, M.: Heliostat Field: computer codes, requirements, comparison of methods. In: Becker, M., Böhmer, M. (Eds.): GAST – The Gas-Cooled Solar Tower Technology Program. Proceedings of the Final Presentation. Springer Verlag, Berlin 1989.

Llorente García I, Álvarez JL, Blanco D. Performance model for parabolic trough solar thermal power plants with thermal storage: Comparison to operating plant data. Solar Energy 2011;85:2443-60.

Patnode A. Simulation and Performance Evaluation of Parabolic Trough Solar Power Plants. Master Thesis. University of Wisconsin-Madison. 2006.

Zaversky F, García-Barberena J, Sánchez M, Astrain D. Probabilistic modeling of a parabolic trough collector power plant – An uncertainty and sensitivity analysis. Solar Energy 2012;86:2128-39.